J. Electrochem. Sci. Eng. ***00(0)*** *(2025) 2979; https://doi.org/10.5599/jese.2979*

Open Access : : ISSN 1847-9286

www.jESE-online.org

Original scientific paper

Exploring the effects of lithium excess on $LiNi_{0.8}Mn_{0.1}Co_{0.1}O_2$ prepared from a commercial $Ni_{0.8}Mn_{0.1}Co_{0.1}(OH)_2$ precursor

Nur Anna Lia[1,2], Muhd Firdaus Kasim[1,3,✉], Kelimah Elong[1,3], Farish Irfal Saaid[1,2], Maziidah Hamidi[1], Lailatul Isti'adzah[1,3], Azira Azahidi[4], Nurul Atikah Mohd Mokhtar[5] and Muhamad Kamil Yaakob[1,2]

[1]*Centre for Functional Materials and Nanotechnology, Institute of Science, Universiti Teknologi MARA, 40450 Shah Alam, Malaysia*

[2]*School of Physics and Material Studies, Faculty of Applied Sciences, Universiti Teknologi MARA, 40450 Shah Alam, Malaysia*

[3]*School of Chemistry and Environment, Faculty of Applied Sciences, Universiti Teknologi MARA, 40450 Shah Alam, Selangor Darul Ehsan, Malaysia*

[4]*Faculty of Applied Sciences, Universiti Teknologi MARA Cawangan Sarawak, 94300 Kota Samarahan, Sarawak, Malaysia*

[5]*Cell and Battery Test & Development, Global Development Campus, Dyson Manufacturing Sdn Bhd, 81400 Senai, Johor, Malaysia*

Corresponding Authors: ✉*muhdfir@uitm.edu.my*

Received: September 8, 2025; Revised: November 12, 2025; Published: December 5, 2025

Abstract

Optimizing the electrochemical performance of nickel-rich cathode materials, specifically $Ni_{0.8}Mn_{0.1}Co_{0.1}(OH)_2$ (NMC811) precursors, involves careful adjustment of several factors, including modification, calcination temperature and lithium content. In this study, we explored the influence of lithium content on the structural, morphological and electrochemical performances of $Li_xNi_{0.8}Co_{0.1}Mn_{0.1}O_2$, by varying 5, 10, 15 and 20 mol.% of Li excess. An appropriate amount of Li was found to suppress cation mixing effectively. Rietveld refinement showed that increasing Li content gradually reduced cation mixing by enhancing the occupancy of Li^+ ions at the 3a sites, thereby hindering Ni^{2+} migration. Although a higher Li addition (20 mol.%) induced a slight lattice contraction, it exhibited the highest c/a ratio (the ratio of the lattice parameters c and a in the layered hexagonal structure), indicative of a well-ordered layered structure. Furthermore, Li exceeded 20 mol.% suppressed the H2/H3 phase transition, contributing to greater structural stability during cycling. While 15 mol.% Li excess achieved the highest initial discharge capacity (185.42 mAh g^{-1} at 0.1 C), 20 mol.% Li excess exhibited superior capacity retention (82.05 % over 80 cycles at 0.1 C). These results demonstrate the critical role of lithium stoichiometry in maintaining structural integrity and electrochemical stability of Ni-rich NMC cathodes, offering valuable insights for the design of high-performance lithium-ion batteries.

Keywords
Lithium-ion battery; Ni-rich cathode materials; Rietveld refinement; cation mixing; NMC

Introduction

The rapid growth of renewable energy sources, such as solar and wind, has heightened global demand for efficient and reliable energy storage technologies. Since these resources are inherently intermittent, large-scale storage systems are essential to maintain grid stability and ensure a continuous energy supply [1,2]. Energy storage solutions, primarily batteries, have gained attention as they play a vital role in stabilizing grids powered increasingly by intermittent renewable sources [3]. Lithium-ion batteries (LIBs) are widely recognized for energy storage due to their high energy density, long cycle life, fast charging capabilities, and cost-effectiveness [4]. In recent years, LIBs have found widespread use in smartphones, electric vehicles (EVs), and hybrid electric vehicles (HEVs). The adoption of EVs, for instance, is recognized as an effective solution to achieve carbon neutrality and mitigate the climate crisis [5,6].

A critical component of LIBs is the cathode material, which largely determines the discharge capacity and lifespan of the battery. Among the various cathode materials explored, nickel-rich lithium nickel manganese cobalt oxides (Ni-rich NMCs) have emerged as a promising class due to their high energy density and reduced dependence on cobalt, a critical raw material with high costs and geopolitical supply risks [7,8]. These cathodes, characterized by a high nickel content (Ni ≥ 60%), offer improved capacity retention and higher energy output compared to lower-nickel compositions. Nevertheless, they also face significant challenges, including structural instability, surface degradation and reactivity with electrolytes, which can lead to capacity fading and safety risks during prolonged cycling [9,10]. These performance limitations are closely linked to cation mixing in their crystal structure. Ni-rich NMCs possess a layered crystal structure in the R-3m space group, in which lithium occupies 3a octahedral sites in the lithium layer and transition metals (Ni, Mn, Co) occupy 3b octahedral sites in the transition-metal layer. Ideally, these layers remain distinct, with minimal cation migration between them. However, due to the similar ionic radii of Li^+ (0.076 nm) and Ni^{2+} (0.069 nm), partial substitution or "mixing" of Ni^{2+} into lithium sites can occur during synthesis or during battery cycling, leading to phase transformations and particle cracking [11,12]. This phenomenon, known as cation mixing or site disorder, negatively affects the electrochemical performance of the material.

As the nickel content in Ni-rich NMC materials increases, the extent of cation mixing also rises, further exacerbating these structural and electrochemical issues. To address these challenges, various strategies have been explored, including modifications to synthesis conditions such as sintering temperature, sintering duration and the use of excess lithium [13–15]. For instance, a study by Truong *et al.* reported that increasing the lithium excess in NMC622 led to a lower initial discharge capacity and lower initial coulombic efficiency in the first cycle but improved capacity retention over extended cycling [16]. This highlights the importance of optimizing lithium content to reduce cation mixing and stabilize the crystal structure of Ni-rich cathodes at high states of charge. Although several studies have explored lithium excess in layered oxide cathode materials, investigations specifically addressing Li content optimization in Ni-rich NMC811 remain limited. This is notable given the material's greater susceptibility to cation disorder, structural degradation, and surface reactivity at high nickel content. Moreover, most previous works employed lab-synthesized precursors, which may complicate the interpretation of results due to variables such as pH control, mixing conditions, and chelating agents. In contrast, the present work uses a commercial $Ni_{0.8}Mn_{0.1}Co_{0.1}(OH)_2$ (NMC811) precursor as the

baseline material to ensure reproducibility and industrial relevance, enabling a clear evaluation of the Li excess effect without uncertainties from precursor synthesis. Although several studies have demonstrated that Li excess can enhance the cycling stability of Ni-rich layered oxides, the optimal Li excess remains composition-dependent and poorly understood. For instance, Abebe *et al*. [15] found 4 % Li excess to be optimal for $Ni_{0.9}Mn_{0.05}Co_{0.05}(OH)_2$ precursor, whereas Truong *et al.* [16] reported that 20 % Li excess enhanced the performance of NMC622. These discrepancies suggest that the required Li stoichiometry may vary with Ni content, yet a systematic investigation on commercial Ni-rich precursors is lacking. Therefore, this work systematically varies the lithium content in a commercial NMC811 precursor to elucidate its influence on crystal structure, morphology, and electrochemical performance. The findings highlight the critical role of lithium stoichiometry in governing the structural integrity and electrochemical stability of NMC811, offering valuable guidance for the rational design of Ni-rich cathodes in next-generation lithium-ion batteries.

Experimental

Synthesis of cathode materials

$LiNi_{0.8}Mn_{0.1}Co_{0.1}O_2$ was synthesized *via* the solid-state method. The precursor powder, $Ni_{0.8}Mn_{0.1}Co_{0.1}(OH)_2$, was obtained from commercial supplies (MSE Supplies). Firstly, anhydrous lithium hydroxide (LiOH) was added to NMC811 precursor powders in the container at a molar ratio of 1.05:1, corresponding to 5 mol.% excess Li. The mixture of LiOH and NMC811 was transferred into a ball-milling jar and ball-milled for 40 minutes over four cycles. Each cycle consisted of 5 minutes of milling at 400 rpm, followed by a 5-minute rest, to obtain a homogeneous powder. The obtained powder was placed in an alumina ceramic boat inside the tube furnace and sintered at 450 ˚C for 5 hours in a dry air atmosphere, followed by grinding and annealing at 780 °C for 15 hours in an oxygen atmosphere. The heating rate during sintering and annealing was 5 °C min^{-1}, while the flow rate of dry air and oxygen gas during heating was 0.5 mL min^{-1}. The final product was ground in a mortar to obtain a fine powder. The prepared samples were stored in an argon-filled glovebox to reduce exposure to moisture and air (O2 < 0.5 ppm, H2O < 0.5 ppm). A similar step was repeated for samples with 10, 15 and 20 mol.% excess Li. These samples with varying Li excess were denoted as 1.05NMC (5 mol.% Li excess), 1.10NMC (10 mol.% Li excess), 1.15NMC (15 mol.% Li excess) and 1.20NMC (20 mol % Li excess). A schematic summary of the solid-state synthesis process is shown in Figure 1.

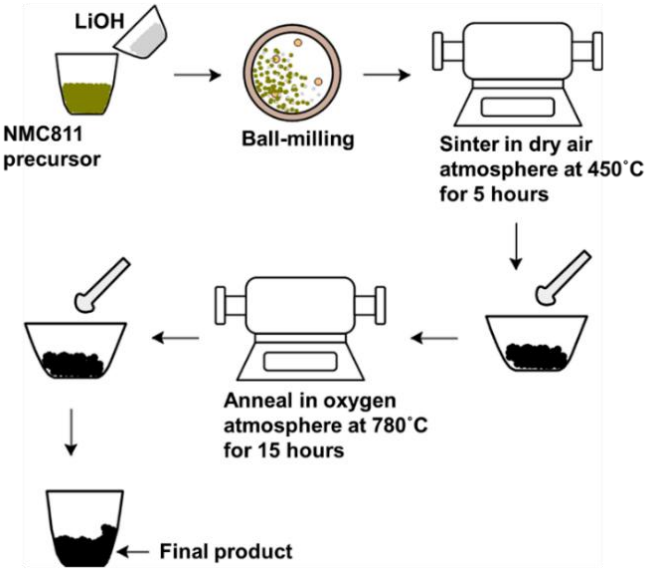

***Figure 1**. Flow of synthesis method*

Characterization

The X-ray diffraction patterns and Rietveld refinement were measured using X-ray diffraction (XRD) to evaluate the qualitative phase analysis and quantitative studies. XRD data was measured by using a PANalytical Xpert Pro Diffraction instrument (Malvern Panalytical, Netherlands) with Cu Kα X-ray radiation operating at 40 kV and 30 mA. The diffraction data were collected from a range of 15 to 90° for a qualitative study and from 15 to 150° for Rietveld refinement. The Rietveld refinement was analysed by using X'pert HighScore Plus software [17] with the structural reference of ICSD 162294. The total occupancy at each crystallographic site was fixed, with transition-metal site ratios (Ni:Mn:Co = 0.8:0.1:0.1) held constant. The background was fitted using a polynomial, and peak profiles were modelled with a pseudo-Voigt function. The morphology and particle size of the materials were studied using field-emission scanning electron microscopy (FESEM, JEOL JSM-7600F, Jeol, Japan) at an acceleration voltage of 3 kV. Element composition and distribution of the element (mapping) of the materials were analysed by using EDX (Oxford INCA X-Max 51-XMX 0021, Oxford Instruments, United Kingdom).

Electrochemical measurements

The cathode composite (active material) consisted of 88 wt.% of NMC811 materials, 6 wt.% of Super-P carbon black and 6 wt.% binder (polyvinylidene fluoride). NMC811, the binder and Super-P were ground first before further processing. The binder was dissolved first in N-Methyl-2-pyrrolidone (NMP) for 3 hours at 50 °C. After 3 hours, Super-P was added and dissolved in the mixing and lastly, the cathode materials were added. The uniform slurry was coated onto 0.02 mm aluminium foils and then dried overnight at 80 °C in a vacuum oven. The dried coating with the electrode thickness approximately 0.12 mm was calendared and cut into circles with a diameter of 15 mm and an electrode area of 1.77 cm^2. The electrode thickness was about 0.10 mm. The loading of the active material and areal capacity were approximately 6-7 mg cm^{-2} and 1.08-1.26 mAh cm^{-2}, respectively. CR2032 coin-type half-cells were assembled in an Ar-filled glove box with NMC811 as the cathode and Li metal as the anode, including the electrolyte solution of 1 M $LiPF_6$ in ethylene carbonate (EC) and dimethyl carbonate (DMC) (EC/DMC, 1:1, v/v; Aldrich); and a microporous polyethylene (PE) membrane as the separator. The WBCS 3000 battery tester (Wonatech, Korea) was used to measure the electrochemical charge-discharge of the cathodes for 80 cycles and rate capability (0.1 C, 0.2 C, 0.5 C, 1 C and 2 C), with a cycling voltage between 2.5 and 4.2 V (0.1 C = 180 mAh g^{-1}). For the rate capability test, the cells were rested for 1 hour between steps. The scan rate in the cyclic voltammetry (CV) tests was controlled at 0.1 mV s^{-1}, with a scan voltage range of 2.3 to 4.5 V. The electrochemical impedance spectroscopy (EIS) measurements were carried out using a WEIS510 Multichannel system (Wonatech, Korea) at an open circuit voltage, temperature of 25.0 ± 0.5 °C, amplitude voltage of 10 mV and the frequency range of 1000 kHz to 0.01 Hz. The EIS data were analysed using Aftermath software by Pine Research Instrumentation.

Results and discussion

Phase and structural studies

Figure 2 shows the structural analysis of all materials. The diffraction peaks can be assigned to a hexagonal α-$NaFeO_2$ crystal structure in the R-3m space group (reference pattern: lithium nickel oxide, 01-089-3601), indicating that the samples are pure and single-phase, with no impurities detected in any of the prepared materials. Upon closer inspection of the XRD patterns, it was observed that increasing the Li content led to distinctive splitting of the (006)/(102) and (018)/(110)

peaks, indicating a highly ordered layered structure [18]. As the lithium content exceeded 5 mol.%, the (003) peak shifted to lower 2θ angles, indicating an increase in the crystal structure's d-spacing due to more Li^+ ions occupying the Li 3a site.

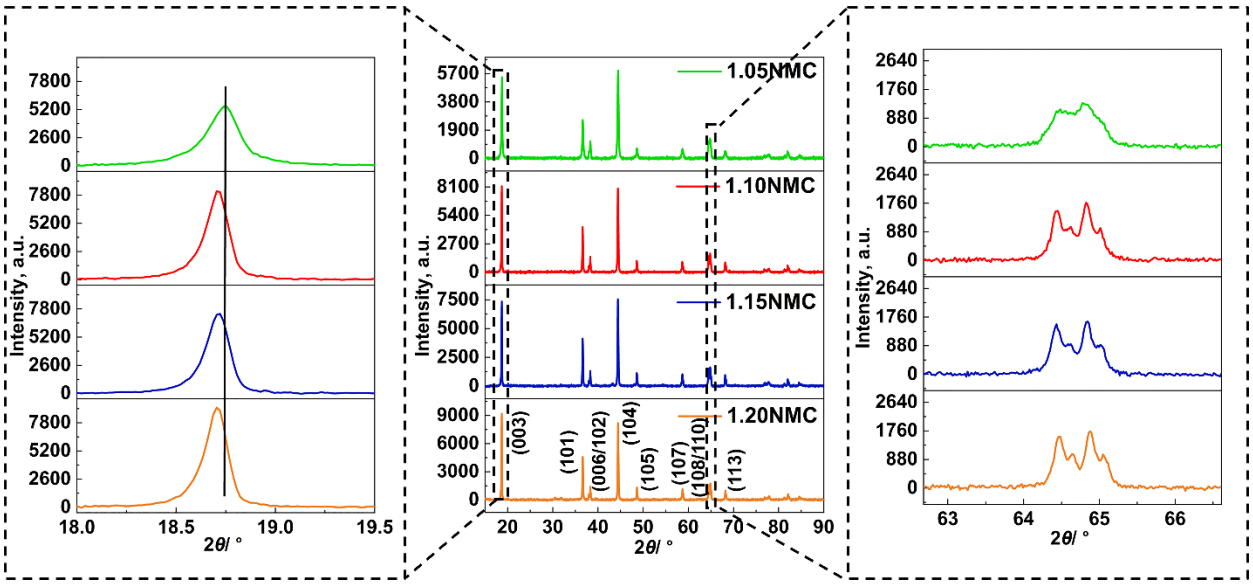

***Figure 2**. XRD profiles and the zoom-in view of the (003) peaks (left) and the (108/110) splitting peaks (right)*

The structure of the materials was further analysed by Rietveld refinement (Figure 3), and the lattice parameters are summarized in Table 1. From Table 1, it can be seen that the c-axis length increases with increasing Li content. This is attributed to more Li+ ions occupying the Li slabs, which causes lattice expansion. A larger c-axis will give benefits to the Li ions diffusion, where more Li^+ ions can participate during the charge/discharge process. A higher c/a ratio (>4.9) also indicates a better layered, well-ordered hexagonal structure in the sample, which is beneficial for enhancing the electrochemical performance of the cathode [14,19]. A moderate Li content was found to suppress cation mixing effectively. This is supported by the refinement results in Table 1, particularly the Ni^{2+} occupancy at the 3a sites. The Ni^{2+} occupancy in 3a sites decreases with increasing Li content, and among them, 1.20NMC shows the lowest Ni^{2+} occupancy in 3a sites [20]. This may be due to the extra Li^+ occupying 3a sites, which reduces the likelihood of Ni^{2+} migration into these positions.

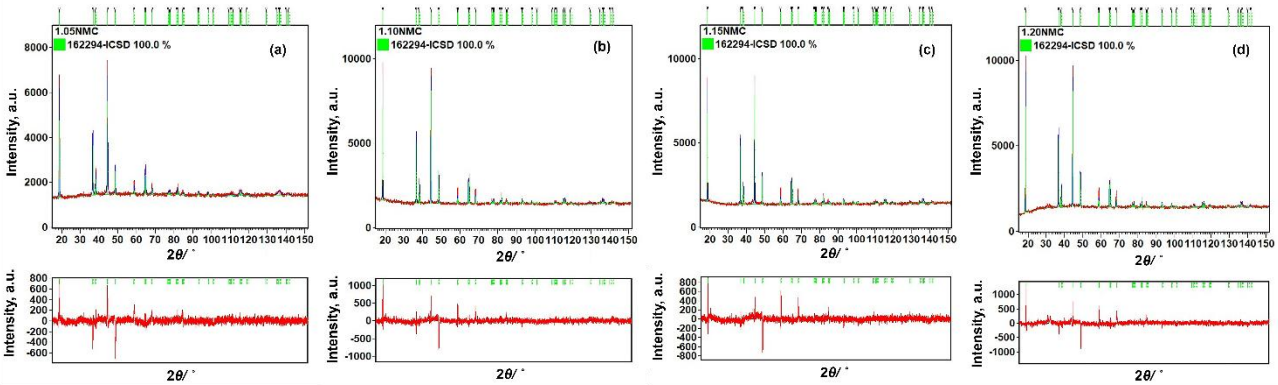

***Figure 3**. Rietveld refinement of a) 1.05NMC, b) 1.10NMC, c) 1.15NMC and d) 1.20NMC*

Meanwhile, 1.05NMC has the highest Ni^{2+} occupancy in the 3a site, having 5.24 %. This suggests that Li loss occurred within the layer structure during sintering and annealing. The 5 mol.% excess Li was insufficient to compensate for the Li loss, resulting in Li deficiency in the cathode material. The Li loss creates more empty space in the Li slab, making it easier for Ni^{2+} to migrate into the 3a

site, thereby leading to a shorter c-axis than in other materials [21]. The Li slab (Li-O) and TM slab (TM-O) thicknesses do not change when the Li content increases by 15 mol.%.

However, when the Li content increased to 20 mol.%, the Li slab and TM slab decreased, correlating with the reduction of the lattice parameters of a and c. Since the occupancy of Ni^{2+} in 3a site is the lowest in 1.20NMC, we assume that the decrease in lattice parameter c is not due to severe cation mixing like 1.05NMC. Instead, this contraction of lattice parameter c is attributed to changes in TM oxidation states, particularly an increase in Ni^{3+} occupancy at 3b sites. Ni^{3+} has a smaller ionic radius (0.056 nm) compared to Ni^{2+} (0.069 nm), thus, this could make the lattice parameter c smaller. Similar observations have been reported in previous studies [21,22]. For instance, Yu *et al*. [21] found that an appropriate amount of Li excess increases the fraction of smaller Ni^{3+} ions, leading to a decrease in lattice parameters and the suppression of Li/Ni cation mixing, thereby stabilizing the layered structure. Although the 1.20NMC sample has smaller lattice parameters compared to 1.10NMC and 1.15NMC, it exhibits the largest *c*/*a* ratio, indicating a more well-ordered layered hexagonal structure.

Table 1. *Crystallographic parameters of the 1.05NMC, 1.10NMC, 1.15NMC and 1.20NMC materials calculated by the Rietveld refinements of the XRD data sets (sof = site of occupancy)*

Sample	R_{wp}	*a* / nm	*c* / nm	*c*/*a*	*V* / nm^3	sof, %		Slab thickness, nm			FWHM
						Ni (3a)	Ni (3b)	Li-O	TM-O	Li-TM	
1.05NMC	3.3737	0.28718	1.41726	4.9351	0.1012235	5.24	74.76	0.1956	0.2122	0.2886	0.19
1.10NMC	3.5688	0.28713	1.41797	4.9384	0.1012387	4.23	75.77			0.2887	0.13
1.15NMC	3.6671	0.28714	1.41852	4.9402	0.1012863	4.17	75.83			0.2888	0.14
1.20NMC	3.9808	0.28687	1.41740	4.9409	0.1010182	2.48	77.52			0.2885	0.13

Morphology and elemental composition analysis

Figure 4 shows the morphology and EDS results for all samples. The average secondary particle size was measured based on 50 particles, and the results are tabulated in Table 2. It was observed that all samples exhibited a similar morphology of spherical secondary particles. All secondary particles in the powders were spherical, with an average size of 7-9 µm. The increase in Li content did not influence the overall particle morphology. The secondary particles were clearly composed of sub-µm-sized primary particles attached together. Based on Table 2, the average particle size grew larger as the Li content increased. The size of the primary particle also increased upon increasing the Li content. Elemental mapping confirmed that all samples have a uniform elemental distribution of Ni, Mn and Co.

Table 2. *Range and average size of secondary particles of 1.05NMC, 1.10NMC, 1.15NMC and 1.20NMC*

Sample	Size of secondary particle, µm	
	Range	Average
1.05NMC	3.562 - 13.031	7.375
1.10NMC	3.701 - 12.426	8.309
1.15NMC	4.476 - 12.530	8.333
1.20NMC	5.725 - 13.614	9.909

Electrochemical performance of cathode materials

To understand the structural transformation and electrochemical reversibility, CV was tested on all materials, and the results are shown in Figure 5a-e. All samples exhibited similar CV curves. In the second cycle, oxidation peaks shifted to lower potentials than in the initial cycle, attributed to the irreversible capacity loss in the first cycle. The well-overlapped reduction peaks of all samples suggest that this irreversible capacity loss originates from the formation of the SEI film [23].

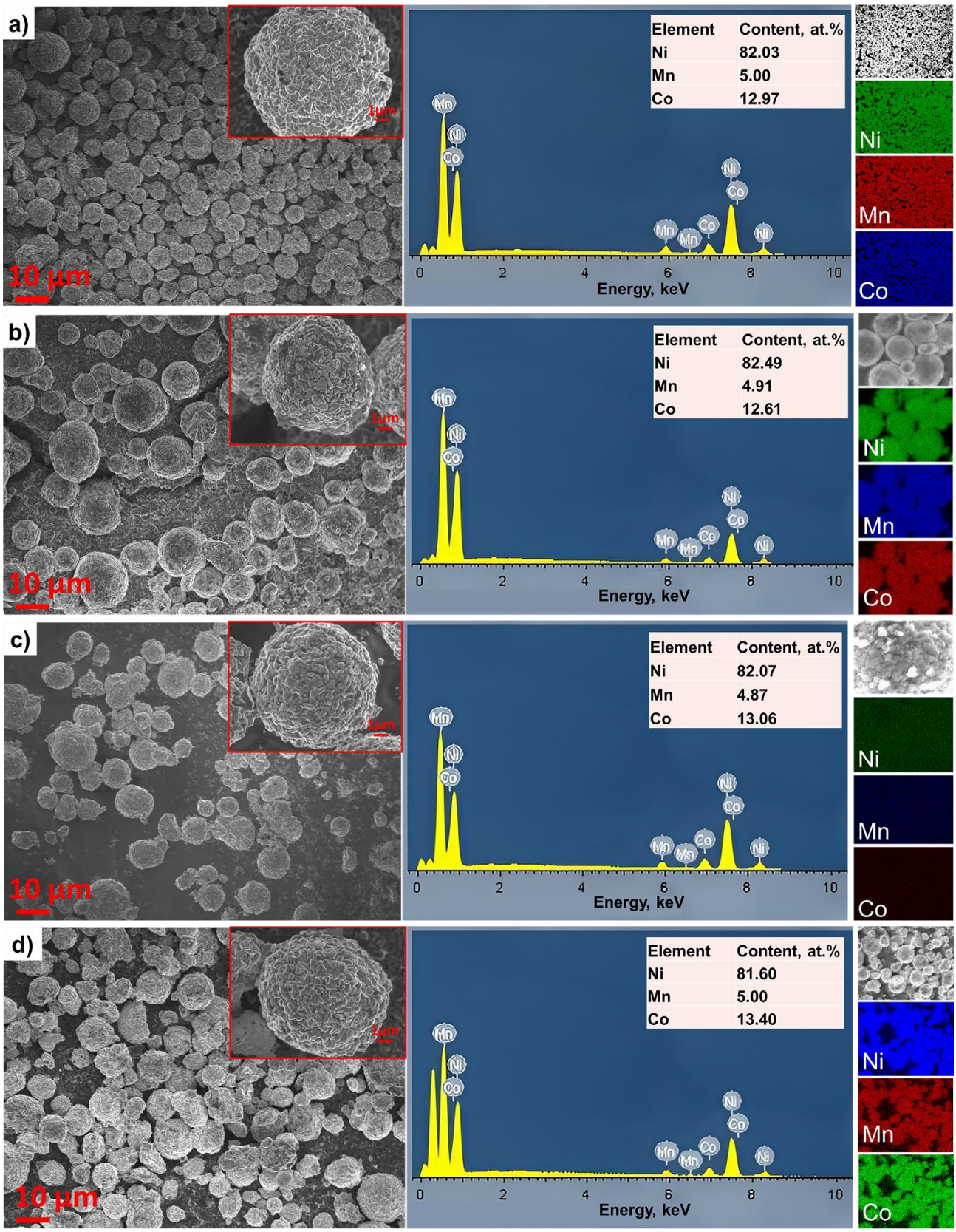

Figure 4. *FESEM images, EDX spectra and elemental mapping of a) 1.05NMC, b), 1.10NMC, c) 1.15NMC and d) 1.20NMC*

The potential differences (Δ*E*) between cathodic and anodic peaks were calculated for the first cycle of all materials to evaluate the degree of polarization. The Δ*E* values for 1.05NMC, 1.10NMC, 1.15NMC and 1.20NMC are 0.290, 0.310, 0.221 and 0.485 V, respectively. Among all materials, the 1.15NMC sample has the lowest Δ*E,* indicating a better rate capability [14].

All samples have phase transitions at three distinct voltages on the electrode. During the Li^+ extraction, Ni-rich materials typically undergo a series of phase transitions, from the original layered structure (H1) to monoclinic phase (M), to the second hexagonal phase (H2) and third hexagonal phase (H3) [24–26]. Commonly, the H2/H3 transition leads to detrimental lattice shrinkage along the c-direction, resulting in structural instability due to volume change and stress accumulation, which can accelerate capacity fading [27]. Increasing the Li content greatly suppressed the intensities of M/H2 and H2/H3. This was confirmed in the 1.20NMC sample, where it shows the weakest H2/H3 transition peak in Figure 5a. The excess Li stabilized the layered structure by reducing lattice distortion. Furthermore, the 1.20NMC sample has a dense and compact lattice structure with a low degree of cation mixing of Ni^{2+} at 3a sites (Table 1), confirming the robustness of this sample, which can make it last longer [28]. The extra Li in the layered structure of 1.20NMC can act as a structural pillar, mitigating volume shrinkage/expansion during cycling, and thereby weakening the H2/H3 phase transition.

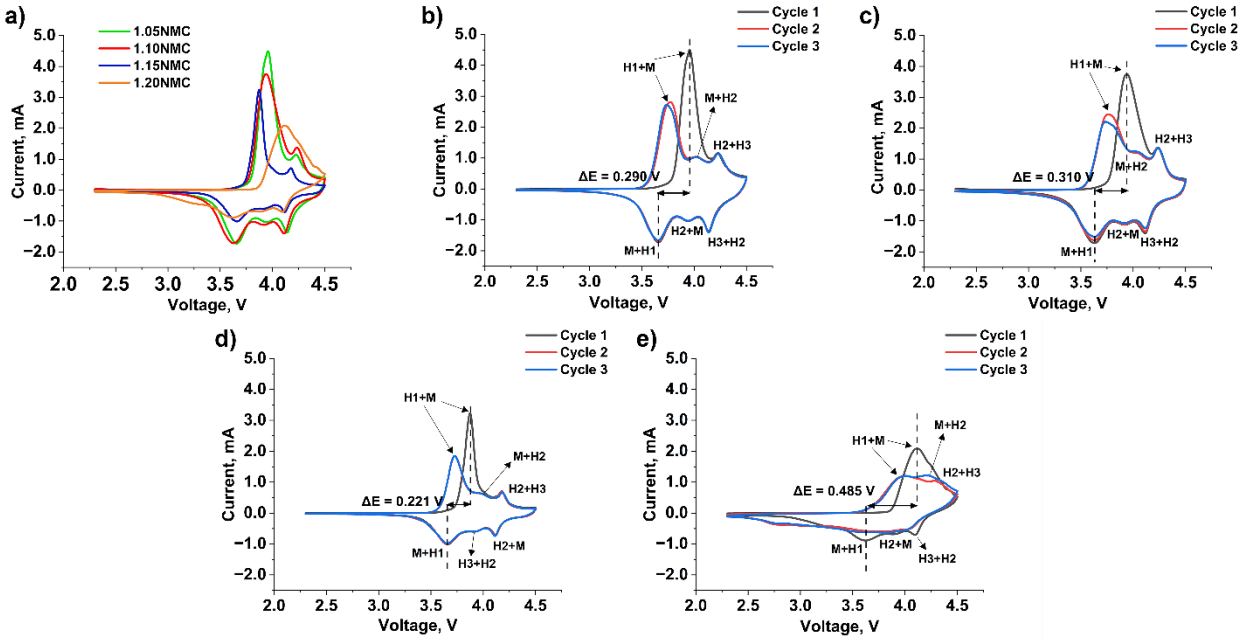

Figure 5. *CV curves of a) all materials for the first cycle, b) 1.05NMC, c) 1.10NMC, d) 1.15NMC and e) 1.20NMC*

Figure 6a-c presents the first charge-discharge curves and cycling performances of all samples at a 0.1 C rate (1 C = 180 mAh g^{-1}). The corresponding results are summarized in Table 3. The initial discharge capacities of 1.05NMC, 1.10NMC, 1.15NMC and 1.20NMC were 163.29, 179.50, 185.42 and 177.65 mAh g^{-1}, respectively. These data reveal that the initial discharge capacity increases with lithium content up to 15 mol % but decreases beyond this level. This trend can be explained by the lattice parameters of the materials (Table 1). As the lithium content increases up to 15 mol %, the c-axis value becomes larger, which is known to facilitate Li^+ movement by promoting more efficient ion diffusion [17]. However, the reduction in initial capacity for 1.20NMC is attributed to its lattice structure. Table 1 shows that 1.20NMC has a smaller c-axis compared to 1.10NMC and the smallest lattice volume among all samples, indicating a more compact crystal structure. Due to this compactness, more energy is required to extract Li^+ ions during charging. This observation is further supported by the CV results (Figure 5a), where the initial oxidation peak for 1.20NMC occurs at a higher voltage than those of other samples, indicating that Li^+ is more tightly bound in the lattice and requires greater energy for removal. Figure 6b also displays the cycling performance of all samples over 80 cycles.

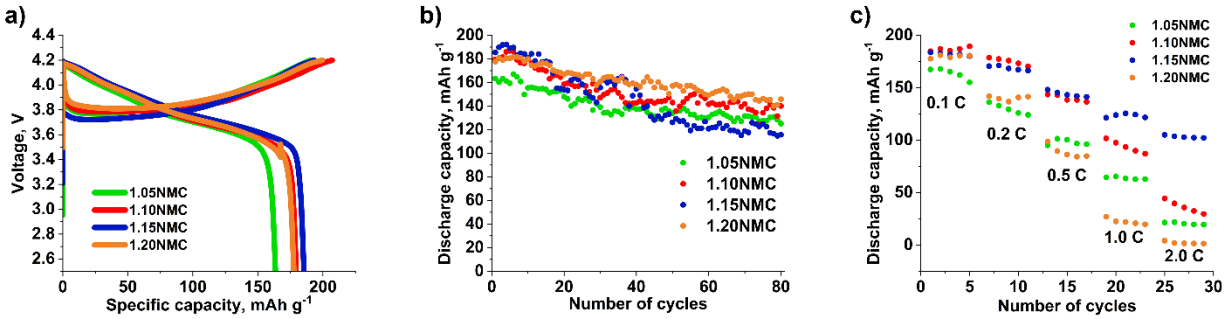

Figure 6. *Electrochemical performance of a) initial discharge capacity, b) cycling performance and c) rate capability of 1.05NMC, 1.10NMC, 1.15NMC and 1.20NMC*

Table 3. *Charge and discharge capacity for 1st, 2nd, and 80th cycle, capacity retention and initial Coulombic efficiency of 1.05NMC, 1.10NMC, 1.15NMC and 1.20NMC*

Sample	Cycle						Capacity retention, %	Initial Coulombic efficiency, %
	1st		2nd		80th			
	Capacity, mAh g-1							
	Charge	Discharge	Charge	Discharge	Charge	Discharge		
1.05NMC	190.61	163.29	158.30	160.29	120.34	125.12	76.62	85.80
1.10NMC	207.14	179.50	183.23	179.50	144.23	140.04	78.02	86.66
1.15NMC	193.20	185.42	173.83	189.86	108.90	115.68	62.39	95.97
1.20NMC	199.42	177.65	183.93	180.93	150.17	145.77	82.05	89.09

Among the samples, 1.20NMC exhibits the highest capacity retention, which is attributed to its excellent structural integrity. This sample features a compact lattice structure with the lowest degree of cation mixing, enhancing its durability during prolonged cycling. Meanwhile, despite having the highest initial discharge capacity, 1.15NMC suffered a faster capacity fading. The inferior electrochemical performance of 1.15NMC compared to 1.20NMC may be attributed to its structural characteristics. The refinement result indicates that 1.15NMC possesses a larger lattice parameter c and broader Li-TM distance, which may initially facilitate Li^+ ions transport. However, this expanded framework weakens interlayer interactions and reduces structural compactness, which is commonly known to stabilize the Li layer (3a site). Such destabilization promotes Ni^{2+} to migrate to the 3a site, consistent with the higher Ni^{2+} occupancy observed in 1.15NMC. The occupancy of Ni^{2+} in the 3a site can gradually migrate to the particle surface due to a low energy barrier, leading to Ni depletion in bulk, structural instability, and capacity loss [29]. In contrast, the denser and more compact lattice of 1.20NMC achieves a favourable balance between slab stabilization and structural robustness, thereby improving capacity retention.

The rate performance of the materials was further evaluated by varying the current rates at 0.1, 0.2, 0.5, 1.0 and 2.0 C, with each sample being tested for 5 cycles. As shown in Figure 6c, the discharge capacity decreased with increasing current density. All materials exhibited gradual capacity fading with increasing current density, presumably due to severe side reactions or electrolyte decomposition at the surface of the active materials, leading to morphological cracking or collapse of the oxide lattice [16]. Although 1.20NMC demonstrated excellent cycling stability for 80 cycles at 0.1 C, it showed the fastest fading capacity with the increase of the current density, as shown in Figure 6c. This rapid capacity fading is due to poor Li^+ extraction/insertion kinetics at higher current rates [14]. Clearly, the rate capability degraded with increasing Li content. Interestingly, 1.15NMC has good rate capability despite having the lowest cycling performance. This suggests that 1.15NMC can undergo fast charge-discharge processes without significant capacity loss or efficiency decline over short-time cycling.

The impedance of 1.05NMC and 1.20NMC, representing low and high lithium content in the NMC precursor, respectively, was further studied using electrochemical impedance spectroscopy (EIS). EIS is a versatile, non-destructive technique for electrochemical measurements, providing deep insights into reaction mechanisms, charge-transfer dynamics, and the resistive and capacitive properties of materials [30]. Impedance data is typically interpreted using equivalent circuit models via fitting. In Nyquist plots, a parallel configuration of an ideal resistor and capacitor produces a semicircle, while a series arrangement of the same components produces a vertical line parallel to the y-axis. A combination of a parallel resistor-capacitor pair with another capacitor in series results in a semicircle followed by a vertical spike [31]. However, in lithium-ion batteries, complexities such as active material inhomogeneity, surface roughness and leakage capacitance cause deviations from these ideal patterns [32].

Figure 7a and 7 b show the Nyquist plots and the corresponding equivalent circuits of 1.05NMC and 1.20NMC, respectively, before and after 80 cycles. The Nyquist plots of fresh 1.05NMC and 1.20NMC samples feature a high-frequency depressed semicircle and a low-frequency tilted spike, as presented in Figure 7a. The equivalent circuit used to fit these plots includes a series resistance (R_s) connected in parallel with the charge-transfer resistance (R_{ct}) and a leaky capacitor/ /constant phase element (CPE), in series with the Warburg impedance (W). The Nyquist plots after 80 cycles of 1.05NMC and 1.20NMC feature two depressed semicircles in the high- and mid-frequency regions and a tilted spike in the low-frequency region, as presented in Figure 7b. The first semicircle corresponds to the impedance of the solid electrolyte interphase (SEI) layer formed at the electrode-electrolyte interface due to electrolyte decomposition during cycling [32], while the second semicircle demonstrates R_c [25] $_t$. The equivalent circuit for these plots comprises a series resistance (R_s) connected to a parallel combination of SEI resistance (R_{sei}) and a CPE, followed by another parallel combination of the R_{ct} and a CPE, with W in series. The fitting results for resistive impedance components are summarized in Table 4. The R_{sei} values of 1.05NMC and 1.20NMC increased from 22.362 to 70.300 Ω due to thick SEI surface layers resulting from the high Li content. Meanwhile, the R_{ct} values of 1.05NMC and 1.20NMC after 80 cycles increased from 122.176 to 241.795 Ω, and 59.272 to 159.472 Ω, respectively. Although 1.20NMC exhibited a higher R_{sei} than 1.05NMC, it maintained a lower of R_{ct} after cycling. Since the electrochemical reaction strongly depends on R_{ct}, a lower R_{ct} corresponds to better electrochemical performance. This result is consistent with the long cycling performance shown in Figure 6b, confirming that an appropriate amount of Li excess in 1.20NMC contributes to enhanced cycling stability.

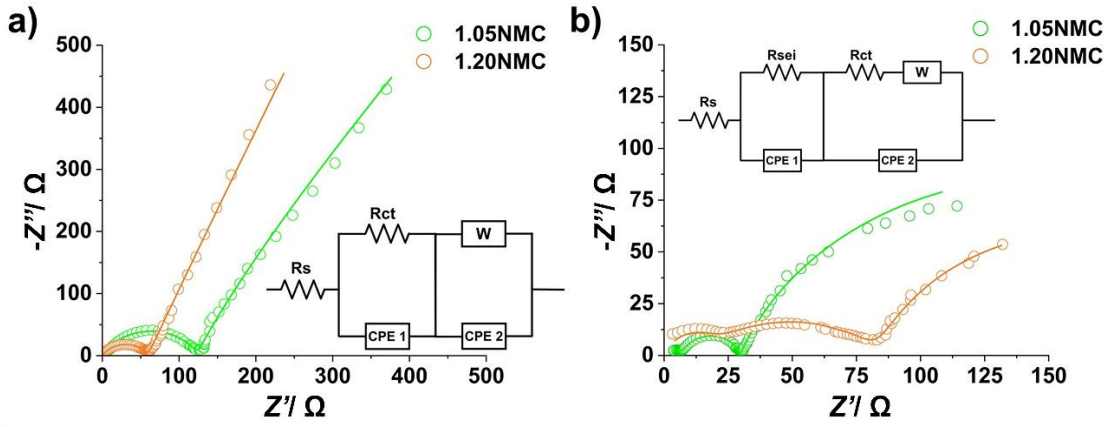

Figure 7. *Nyquist plots and equivalent circuit of 1.05NMC and 1.10NMC: a) before cycling and b) after 80th cycle*

Table 4. *EIS fitting results for 1.05NMC and 1.20NMC*

Sample	Before cycling		After 80th cycling	
	1.05NMC	1.20NMC	1.05NMC	1.20NMC
R_s / Ω	1.761	0.377	0.852	0.181
R_{sei} / Ω	-	-	22.362	70.300
R_{ct} / Ω	122.176	59.272	241.795	159.472

The electrochemical performance of NMC811 cathodes with varying lithium content was compared with results from previous studies, as summarized in Table 5. The findings indicate that an appropriate lithium excess in layered cathode materials effectively suppresses cation disorder, enhances structural stability, and facilitates Li-ion transport, thereby improving capacity retention. Furthermore, each NMC composition exhibits a distinct optimal level of Li excess, underscoring the need for composition-specific optimization to achieve optimal electrochemical performance. Notably, our 1.20NMC sample exhibits low cation mixing and excellent electrochemical performance in NMC811, which highlights that the beneficial effect of Li content is not simply proportional but depends on an optimized range.

Table 5. *Comparison of the electrochemical performance of Li excess on Ni-rich cathode materials done by the previous studies (Precursor synthesis method: co-precipitation, except for commercial precursor)*

Starting materials	Cathode materials	Range of Li excess, mol.%	Li excess, mol.%	Capacity*, mAh g^{-1} @C-rate	Capacity retention, % @cycle number	Cut-off voltage, V	Highlight	Ref.
$NiSO_4·6H_2O$ $CoSO_4·7H_2O$ $MnSO_4·H_2O$	$LiNi_{0.9}Mn_{0.05}Co_{0.05}O_2$	0, 2, 4, 6, 8	4	216.17 @ 0.1 C	95.79 @ 200	2.7 to 4.3	• The optimal Li excess improved rate performance and structural stability due to enhance crystal-linity and reduced cation mixing. • A moderate Li excess improved structural stability and electro-chemical performance of cathode material.	[15]
$NiSO_4·6H_2O$, $CoSO_4·7H_2O$, $MnSO_4·H_2O$	$LiNi_{0.6}Mn_{0.2}Co_{0.2}O_2$	5, 10, 20, 25	20	181.3 @ 0.1 C	90.0 @ 200	2.8 to 4.5	• Improve thermal stability, preventing thermal runaway • Cation mixing occurred with increased of Li excess, affecting lattice parameters and structural stability	[16]
Commercial precursor $Ni_{0.88}Mn_{0.06}$- $-Co_{0.06}(OH)_2$	$LiNi_{0.88}Mn_{0.06}Co_{0.06}O_2$	3, 6, 9, 12	6	209.1 @ 0.1 C	91.70 @ 100	3.0 to 4.3	• Less Li-excess leads to low cycling stability and inferior rate performance due to poor crystallinity and microcracks during cycling • Proper Li excess enhances structural stability, particle sizes, and electrochemical performance	[21]
$NiSO_4$, $CoSO_4$	$LiNi_{0.8}Co_{0.2}O_2$	10, 20	10	222.0 @ 0.1 C	85.0 @ 200	2.7 to 4.5	• Increased of Li/Ni exchange ratio and Li slab space with Li-enrichment. • Excessive Li/Ni exchange led to capacity fading and structural collapse during electrochemical cycling	[29]
$NiSO_4$, $MnSO_4$, $CoSO_4$	$LiNi_{0.8}Mn_{0.1}Co_{0.1}O_2$	10, 20, 30	20	195.3 @ 0.2 C	77.3 @ 100	2.7 to 4.6	• The morphology of samples shows less compactness with increased Li source • Increased Li content enhances Ni^{2+} and improves cycling stability and rate capability	[33]
Commercial precursor $Ni_{0.80}Mn_{0.10}$- $-Co_{0.10}(OH)_2$	$LiNi_{0.8}Mn_{0.1}Co_{0.1}O_2$	5, 10, 15, 20	20	177.65 @ 0.1 C	82.05 @ 80	2.5 to 4.2	• Increased Li content, reduced cation mixing • H2/H3 phase transition can be suppressed when Li content increased, thereby improve the cycling performance	This study

*1st cycle

Our results demonstrate that 1.20NMC provides the most balanced performance in our system, highlighting the need for optimizing Li stoichiometry depending on the targeted application and processing conditions.

Conclusions

A well-ordered layer-structured $LiNi_{0.8}Mn_{0.1}Co_{0.1}O_2$ was successfully synthesized using the solid-state method. The effect of the Li excess on NMC811 was systematically investigated. The secondary particle size of NMC811 increased with the higher Li content. The initial discharge capacity rose as the Li content in NMC811 increased up to 15 mol.%, but decreased at 20 mol.% excess due to the lattice contraction. The capacity retention of the cathode materials improved as the Li content increased, with 1.20NMC exhibiting the highest capacity retention. Among all samples, 1.20NMC showed the weakest H2/H3 phase transition, leading to a more stable layered structure during charge/discharge. However, due to the highest degree of polarization arising from H2/H3 suppression, it has poor rate performance. In contrast, 1.15NMC achieved the highest initial discharge capacity of 185.42 mAh g^{-1} but suffered from the lowest capacity retention. Nevertheless, its lowest polarization effect on the layered structure enabled it to exhibit excellent rate capability compared to other samples. These results indicate that 1.20NMC is more suitable for long-term cycling at low current densities, whereas 1.15NMC performs better under high-rate conditions, enabling rapid charge/discharge without significant capacity loss over shorter cycles.

Acknowledgments: *The authors would like to thank the Ministry of Higher Education through the Fundamental Research Grant Scheme (FRGS) with code FRGS/1/2022/STG04/UITM/02/14, Faculty of Applied Sciences and Centre for Functional Materials and Nanotechnology, Institute of Science, Universiti Teknologi MARA, Shah Alam, Selangor, Malaysia for their support to this work.*

Conflicts of Interest: *The authors declare that they have no known competing financial interests or personal relationships that could have appeared to influence the work reported in this paper.*

References

[1] T.-Z. Ang, M. Salem, M. Kamarol, H. S. Das, M. A. Nazari, N. Prabaharan, A comprehensive study of renewable energy sources: Classifications, challenges and suggestions, *Energy Strategy Reviews* **43** (2022) 100939. https://doi.org/10.1016/j.esr.2022.100939

[2] M. Z. Najihah, F. I. Saaid, I. M. Noor, H. J. Woo, T. Winie, Iron cobalt selenide counter electrode for application in dye-sensitized solar cell: synthesis parameter, structural, electrochemical, and efficiency studies, *Ionics (Kiel)* **30** (2024) 2939-2955. https://doi.org/10.1007/s11581-024-05462-z

[3] Q. Hassan, P. Viktor, T. J. Al-Musawi, B. Mahmood Ali, S. Algburi, H. M. Alzoubi, A. Khudhair Al-Jiboory, A. Zuhair Sameen, H. M. Salman, M. Jaszczur, The renewable energy role in the global energy Transformations, *Renewable Energy Focus* **48** (2024) 100545. https://doi.org/10.1016/j.ref.2024.100545

[4] K. R. Ngoy, V. T. Lukong, K. O. Yoro, J. B. Makambo, N. C. Chukwuati, C. Ibegbulam, O. Eterigho-Ikelegbe, K. Ukoba, T.-C. Jen, Lithium-ion batteries and the future of sustainable energy: A comprehensive review, *Renewable and Sustainable Energy Reviews* **223** (2025) 115971. https://doi.org/10.1016/j.rser.2025.115971

[5] T. Kim, W. Song, D. Y. Son, L. K. Ono, Y. Qi, Lithium-ion batteries: outlook on present, future, and hybridized technologies, *Journal of Materials Chemistry A* **7** (2019) 2942-2964. https://doi.org/10.1039/C8TA10513H

[6] A.M. Ralls, K. Leong, J. Clayton, P. Fuelling, C. Mercer, V. Navarro, P.L. Menezes, The Role of Lithium-Ion Batteries in the Growing Trend of Electric Vehicles, *Materials* **16** (2023) 6063. https://doi.org/10.3390/ma16176063

[7] L. Yu, T. Liu, R. Amine, J. Wen, J. Lu, K. Amine, High Nickel and No Cobalt-The Pursuit of Next-Generation Layered Oxide Cathodes, *ACS Applied Materials & Interfaces* **14** (2022) 23056-23065. https://doi.org/10.1021/acsami.1c22091

[8] S..D. William Gourley, T. Or, Z. Chen, Breaking Free from Cobalt Reliance in Lithium-Ion Batteries, *iScience* **9** (2020) 101505. https://doi.org/10.1016/j.isci.2020.101505

[9] H. Cho, J. Kim, M. Kim, H. An, K. Min, K. Park, A review of problems and solutions in Ni-rich cathode-based Li-ion batteries from two research aspects: Experimental studies and computational insights, *Journal of Power Sources* **597** (2024) 234132. https://doi.org/10.1016/j.jpowsour.2024.234132

[10] W. Kim, S. Park, G. Ko, K. Kwon, The effects of Fe/Al co-modified Ni-rich $Li[Ni_{1-x-y}Co_xMn_y]O_2$ for enhancing electrochemical performance, *Journal of Physics and Chemistry of Solids* **170** (2022) 110925. https://doi.org/10.1016/j.jpcs.2022.110925

[11] J. Li, G. Liang, W. Zheng, S. Zhang, K. Davey, W. K. Pang, Z. Guo, Addressing cation mixing in layered structured cathodes for lithium-ion batteries: A critical review, *Nano Materials Science* **5** (2023) 404-420. https://doi.org/10.1016/j.nanoms.2022.09.001

[12] W. A. H. W. Azizan, K. Elong, M. F. Kasim, *Effect of Al doped in Ni-rich $LiNi_{0.6}Co_{0.3}Ti_{0.1}O_2$ cathode materials and their electrochemical performance for rechargeable lithium-ion batteries*, *Materialstoday: Proceedings* **52(2)** (2022) 1399-1403 https://doi.org/10.1016/j.matpr.2021.11.530.

[13] L. Tang, X. Cheng, R. Wu, T. Cao, J. Lu, Y. Zhang, Z. Zhang, Monitoring the morphology evolution of $LiNi_{0.8}Mn_{0.1}Co_{0.1}O_2$ during high-temperature solid state synthesis via in situ SEM, *Journal of Energy Chemistry* **66** (2022) 9-15.https://doi.org/10.1016/j.jechem.2021.07.021

[14] J. T. Zhang, X. H. Tan, L. M. Guo, Y. Jiang, S. N. Liu, H. F. Wang, X. H. Kang, W. G. Chu, Controllable formation of lithium carbonate surface phase during synthesis of nickel-rich $LiNi_{0.9}Mn_{0.1}O_2$ in air and its protection role in electrochemical reaction, *Journal of Alloys and Compounds* **771** (2019) 42-50. https://doi.org/10.1016/j.jallcom.2018.08.243

[15] E. B. Abebe, C. C. Yang, S. H. Wu, W. C. Chien, Y. J. J. Li, Effect of Li Excess on Electrochemical Performance of Ni-Rich $LiNi_{0.9}Co_{0.05}Mn_{0.05}O_2$ Cathode Materials for Li-Ion Batteries, *ACS Applied Energy Materials* **4** (2021) 14295-14308. https://doi.org/10.1021/acsaem.1c03004

[16] B. T. T. Truong, Y. S. Wu, T. F. Hung, W. C. Chien, S. H. Wu, R. Jose, S. J. Lue, C. C. Yang, The effect of lithium-excess on Ni-rich $LiNi_{0.6}Co_{0.2}Mn_{0.2}O_2$ cathode materials prepared by a Taylor flow reactor, *Electrochimica Acta* **391** (2021). https://doi.org/10.1016/j.electacta.2021.138982

[17] M.F. Kasim, W.A.H.W. Azizan, K.A. Elong, N. Kamarudin, M.K. Yaakob, N. Badar, Enhancing the structural stability and capacity retention of Ni-rich $LiNi_{0.7}Co_{0.3}O_2$ cathode materials via Ti doping for rechargeable Li-ion batteries: Experimental and computational approaches, *Journal of Alloys and Compounds* **888** (2021) 161559. https://doi.org/10.1016/j.jallcom.2021.161559.

[18] R. Santhanam, P. Jones, A. Sumana, B. Rambabu, Influence of lithium content on high rate cycleability of layered $Li_{1+x}Ni_{0.30}Co_{0.30}Mn_{0.40}O_2$ cathodes for high power lithium-ion batteries, *Journal of Power Sources* **195** (2010) 7391-7396 https://doi.org/10.1016/j.jpowsour.2010.06.004

[19] R. D. Nanda, S. A. Kristianto, E. Kartini, M. Fakhrudin, The Effect of Lithium Excess on NMC-721 using Oxalate Co-precipitation, *Journal of Batteries for Renewable Energy and Electric Vehicles* **1** (2023) 23-27. https://doi.org/10.59046/jbrev.v1i01.7

[20] H. Li, H. Liu, S. Luo, J. Arbiol, E. Suard, T. Bergfeldt, A. Missyul, V. Baran, S. Mangold, Y. Zhang, W. Hua, M. Knapp, H. Ehrenberg, F. Pan, S. Indris, Author Correction: Tuning Li occupancy and local structures for advanced Co-free Ni-rich positive electrodes, *Nature Communications* **16** (2025) 3577. https://doi.org/10.1038/s41467-025-58942-9

[21] Z. Yu, X. Qu, T. Wan, A. Dou, Y. Zhou, X. Peng, M. Su, Y. Liu, D. Chu, Synthesis and Mechanism of High Structural Stability of Nickel-Rich Cathode Materials by Adjusting Li-Excess, *ACS Applied Materials & Interfaces* **12** (2020) 40393-40403. https://doi.org/10.1021/acsami.0c12541.

[22] D. Rathore, C. Liang, E. Zsoldos, M. Ball, S. Yu, C. Yang, Q. Wang, J.R. Dahn, Elucidating the Role of Excess Li in the Electrochemical Performance of $Li_{1+x}[Ni_{0.5}Mn_{0.5}]_{1-x}O_2$ Layered Oxides, *Journal of The Electrochemical Society* **170** (2023) 020520. https://doi.org/10.1149/1945-7111/acb852

[23] J. Zhang, Z. Yang, R. Gao, L. Gu, Z. Hu, X. Liu, Suppressing the Structure Deterioration of Ni-Rich $LiNi_{0.8}Co_{0.1}Mn_{0.1}O_2$ through Atom-Scale Interfacial Integration of Self-Forming Hierarchical Spinel Layer with Ni Gradient Concentration, *ACS Applied Materials & Interfaces* **9** (2017) 29794-29803. https://doi.org/10.1021/acsami.7b08802

[24] L. Qiao, Q. You, X. Wu, H. Min, X. Liu, H. Yang, Mo Doping to Modify Lattice and Morphology of the $LiNi_{0.9}Co_{0.05}Mn_{0.05}O_2$ Cathode toward High-Efficient Lithium-Ion Storage, *ACS Applied Materials & Interfaces* **16** (2024) 4772-4783. https://doi.org/10.1021/acsami.3c16475.

[25] B. Jeevanantham, M.K. Shobana, S.A. Ahmed, Y.-P. Fu, W.-N. Su, B.J. Hwang, Improving high-voltage cycling and stabilizing the electrode-electrolyte interface of nickel-rich layered cathodes by magnesium doping, *Journal of Physics and Chemistry of Solids* **195** (2024) 112296. https://doi.org/10.1016/j.jpcs.2024.112296

[26] S. H. Song, S. Hong, M. Cho, J.G. Yoo, H. Min Jin, S. H. Lee, M. Avdeev, K. Ikeda, J. Kim, S. C. Nam, S. H. Yu, I. Park, H. Kim, Rational design of Li off-stoichiometric Ni-rich layered cathode materials for Li-ion batteries, *Chemical Engineering Journal* **448** (2022) 137685. https://doi.org/10.1016/j.cej.2022.137685

[27] J. Chen, H. Yang, T. Li, C. Liu, H. Tong, J. Chen, Z. Liu, L. Xia, Z. Chen, J. Duan, L. Li, The Effects of Reversibility of H2-H3 Phase Transition on Ni-Rich Layered Oxide Cathode for High-Energy Lithium-Ion Batteries, *Frontiers in Chemistry* **7** (2019) 500. https://doi.org/10.3389/fchem.2019.00500

[28] Z. Zhao, C. Li, Z. Wen, Z. Yang, S. Lu, X. Zhang, S. Chen, B. Wu, F. Wu, D. Mu, Cation mixing effect regulation by niobium for high voltage single-crystalline nickel-rich cathodes, *Chemical Engineering Journal* **461** (2023) 142093. https://doi.org/10.1016/j.cej.2023.142093

[29] R. Wang, G. Qian, T. Liu, M. Li, J. Liu, B. Zhang, W. Zhu, S. Li, W. Zhao, W. Yang, X. Ma, Z. Fu, Y. Liu, J. Yang, L. Jin, Y. Xiao, F. Pan, Tuning Li-enrichment in high-Ni layered oxide cathodes to optimize electrochemical performance for Li-ion battery, *Nano Energy* **62** (2019) 709-717. https://doi.org/10.1016/j.nanoen.2019.05.089

[30] B. Padha, S. Verma, P. Mahajan, S. Arya, Electrochemical Impedance Spectroscopy (EIS) Performance Analysis and Challenges in Fuel Cell Applications, *Journal of Electrochemical Science and Technology* **13** (2022) 167–176. https://doi.org/10.33961/jecst.2021.01263.

[31] F. Saaid, I. Rodi, T. Winie, Effect of temperature on the transport property of PVdF-HFP-MPII-PC/DME gel polymer electrolytes, *AIP Conference Proceedings* **1877(1)** (2017) 020006. https://doi.org/10.1063/1.4999856

[32] W. Choi, H. C. Shin, J. M. Kim, J. Y. Choi, W. S. Yoon, Modeling and applications of electrochemical impedance spectroscopy (Eis) for lithium-ion batteries, *Journal of Electrochemical Science and Technology*. **11** (2020) 1-13. https://doi.org/10.33961/jecst.2019.00528

[33] F. Wu, J. Tian, Y. Su, J. Wang, C. Zhang, L. Bao, T. He, J. Li, S. Chen, Effect of Ni 2+ Content on Lithium/Nickel Disorder for Ni-Rich Cathode Materials, *ACS Applied Materials & Interfaces* **7** (2015) 7702-7708. https://doi.org/10.1021/acsami.5b00645